

Facile and green synthesis of Co_3O_4 nanoplates/graphene nanosheets composite for supercapacitor

Xiwen Wang · Suqin Liu · Haiyan Wang · Feiyue Tu · Dong Fang · Yanhua Li

Received: 13 February 2012 / Revised: 29 March 2012 / Accepted: 4 April 2012 / Published online: 14 June 2012
© Springer-Verlag 2012

Abstract A series of Co_3O_4 nanoplates/graphene nanosheets (GNS) composites are fabricated using a facile and green method by hydrothermal treatment and subsequent calcinations in air. The Co_3O_4 nanoplates with a length of 0.5–1 μm and width of 100–300 nm are homogeneously distributed on the surface of graphene nanosheets which are reduced under mild hydrothermal treatment as investigated by X-ray diffraction, scanning electron microscopy, and transmission electron microscopy. Electrochemical properties are tested by cyclic voltammetry, galvanostatic charge–discharge, and electrochemical impedance spectroscopy. The Co_3O_4 nanoplates/7.0 % GNS composite shows a maximum specific capacitance of 667.9 Fg^{-1} at 1.25 A g^{-1} and 412.5 Fg^{-1} at 5 A g^{-1} in 2 M KOH aqueous solution. The composite exhibits excellent cycling stability with 18.7 % of specific capacitance increased after 1,000 cycles.

Keywords Graphene nanosheets · Cobalt oxide nanoplates · Hydrothermal method · Composite · Supercapacitor

X. Wang · S. Liu (✉) · H. Wang · F. Tu · D. Fang · Y. Li
College of Chemistry and Chemical Engineering,
Central South University,
Changsha 410083, China
e-mail: suqinliu2003@126.com

D. Fang
Key Lab of Green Processing and Functional Textiles of New
Textile Materials, Ministry of Education,
Wuhan Textile University,
Wuhan 430073, China

Y. Li
Department of Chemical Engineering and Information
Engineering, Changsha Aeronautical Vocational
and Technical College,
Changsha, Hunan 410124, China

Introduction

Recently, tremendous attention has been focused on pseudocapacitors, which proceed with reversible faradic redox reaction of materials including transition metal oxides, transition metal hydroxides, and conducting polymers due to their high power density and long cycle life [1–4]. However, the energy density of pseudocapacitors is still low. A novel strategy incorporating nanostructured carbon materials, such as porous carbon sphere [5, 6], carbon nanotube [7–9], carbon fiber [10, 11], and graphene [12–15], has been employed to address the issue and improve the conductivity of electrode materials as well.

Since the isolation of single-layer graphene in 2004 [16], graphene has attracted much attention due to the theoretical special surface area of 2,630 $\text{m}^2 \text{g}^{-1}$, the high intrinsic electric conductivity, as well as the excellent mechanical strength and chemical stability. Graphene and graphene-based materials have been explored for lithium ion batteries, fuel cells, solar cells, and supercapacitors [17–20]. However, the serious agglomeration and restacking of graphene nanosheets (GNS) result in great specific surface area loss and consequently a lower capacitance than the anticipated value. For example, Ruoff and co-workers have reported graphene-based supercapacitor with specific capacitance of 166 and 135 Fg^{-1} in ion liquid [21] and aqueous solution [22], respectively. Researchers have been committed to construct a flexible interleaved structure with transition metal nanostructure attached to GNS to boost the capacitive performance of graphene-based materials, such as GNS– Mn_3O_4 [23], GNS– MnO_2 [24, 25], GNS– ZnO [26], GNS– SnO_2 [27], and GNS– Co_3O_4 [28]. Among the transition metal oxides, Co_3O_4 is found to be one of the most promising electrode materials because of high redox activity, great reversibility, and theoretical special capacitance of 3,580 Fg^{-1} [29]. Although there are

some reports on the preparation of GNS–Co₃O₄, the strategies are not environmental in which graphene nanosheets is reduced using hydrazine [30] or NaBH₄ [31]. It is well known that these reduction agents are toxic, explosive, and expensive. Therefore, synthesis of GNS-based materials with a facile and environment-friendly approach is still a big challenge.

In this work, we propose a facile and green method for growing cobalt oxide nanoplates on graphene nanosheets. Under hydrothermal treatment, the exfoliated graphite oxide (GO) is reduced, and simultaneously cobalt hydroxide is deposited on the surface of GNS. A sequence of Co₃O₄ nanoplates/GNS composites is formed by thermal decomposition of cobalt hydroxide/GNS composite. Morphology and electrochemical capacitive performance of Co₃O₄/GNS composite were investigated in detail and the formation mechanism of the nanostructure was also investigated.

Experiment

Preparation of Co₃O₄ nanoplates/GNS composite

GO was prepared from flake graphite powder (500 mesh) by Hummers method as described previously [32]. Typically, as-prepared GO sample (0.5 g) was soaked in an aqueous solution of tetramethylammonium hydroxide (TMAOH) (100 mL, 0.5 mol L⁻¹) for a week. The brown suspension was then dialyzed with deionized water until the pH was 7 and dried in oven at 60 °C for 12 h.

A certain amount (40, 80, 240 mg) of TMAOH-soaked GO was well dispersed in 80 mL deionized water by ultrasonic agitation for 2 h. Cobalt nitrate hexahydrate, urea, and sodium citrate were dissolved in GO dispersion step by step in intervals of 10 min under vigorous stirring to give the final concentration of 40, 80, and 8 mmol L⁻¹, respectively. The dark homogeneous solution was transferred into a 100-mL Teflon-lined stainless steel autoclave. The autoclave was heated at 180 °C for 24 h. The black products deposited at the bottom were washed by centrifugation for three times using deionized water, dried in an oven at 60 °C for 12 h, and then annealed at 350 °C for 3 h in air to form final products. The pure Co₃O₄ nanoplates were synthesized by the previously mentioned steps without the addition of GO.

For comparison, GNS were prepared via a hydrothermal method as reported by Xu and co-workers [33]. A total of 30 mL homogeneous GO aqueous dispersion (1 mg mL⁻¹) was sealed in 50-mL Teflon-lined stainless steel autoclave and hydrothermally treated at 180 °C for 12 h. The cylinder-like graphene hydrogel was collected and dried in vacuum freeze-drying step.

Materials characterization

The crystal structure was determined by X-ray diffractometer (XRD, Rigaku D/max 2550VB⁺) from 5 ° to 70 ° with CuK α radiation ($\lambda=1.54056$ Å). The surface morphology was characterized by scanning electron microscope (SEM; JEOL JSM-6360 LV), transmission electron microscope (TEM; JEOL JEM-2100 F), and atom force microscope (AFM; Veeco Dimension). The Fourier transform infrared (FT-IR) spectra were recorded on Nicolet560 spectroscopy with KBr pellet technique. Raman spectra were tested with Dior LABRAM-1B instrument. The graphene content of GNS/Co₃O₄ composites was measured by C-S800-infrared-carbon sulfur analyzer. The graphene content of as-prepared composites adding 40, 80, and 240 mg GO were determined to be 4.1, 7.0, and 12.3 %, respectively.

Electrochemical measurement

Cycle voltammetry (CV) test, galvanostatic charge–discharge (CD) test, and electrochemical impedance spectroscopy (EIS) were carried out on a CHI660C electrochemistry workstation. The working electrode was prepared by mixing 85 wt.% active materials, 10 wt.% acetylene black as conductive agent, and 5 wt.% poly(tetrafluoroethylene) (PTFE) as binder to form a slurry and pressing the slurry onto a nickel grid (1 cm²). The electrodes were dried under vacuum at 110 °C for 12 h. To fabricate the graphene working electrode, freeze-dried graphene hydrogel was mixed with PTFE in a mass ratio of 95:5. The fabrication of electrode is just the same as detailed earlier. All electrochemical measurements were finished in a three-compartment cell: a working electrode, a platinum plate as counter-electrode, and a saturated calomel electrode (SCE) as reference electrode. The electrolyte was 2 M KOH aqueous solution.

Results and discussion

Microstructure characterizations

Figure 1 shows the XRD patterns of GO, GNS, and Co₃O₄ nanoplates/GNS composite. The intense peak of GO at $2\theta \approx 11^\circ$ corresponds to the (001) reflection. GO exhibits a layered structure with a higher d-spacing (0.806 nm) than that of natural graphite (0.336 nm), which demonstrates complete oxidation of graphite into graphite oxide [34]. For GNS, the (001) peak at 11° disappears and a broad (002) peak appears at 23.6° , confirming the conversion of GO to graphene. Diffraction lines, assigned to the crystal planes of (111), (220), (311), (222), (400), (422), (511), and (440), are observed for the 7 % GNS/Co₃O₄ composite, which are well indexed to face-centered cubic structured as

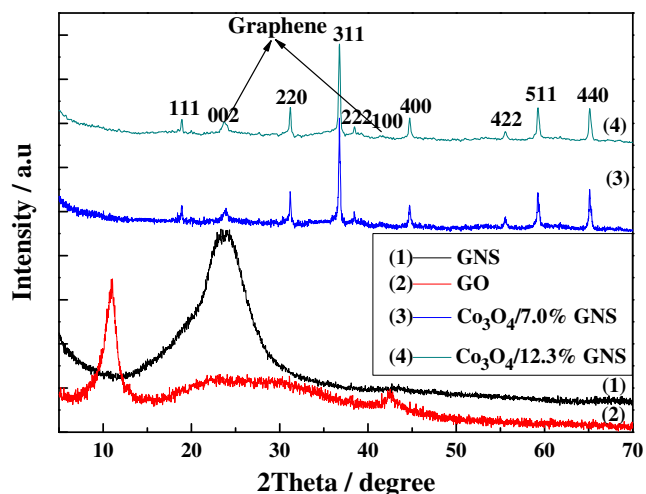


Fig. 1 XRD patterns of GNS, GO, $\text{Co}_3\text{O}_4/7.0\%$ GNS composite, and $\text{Co}_3\text{O}_4/12.3\%$ GNS composite

Co_3O_4 (JCPDS card no. 43–1003, $\text{Fd}3\text{m}$, $a_0=0.808$ nm). The additive peaks at 28.3° (002) and 41.5° (100) can be attributed to graphene. The (002) peak and (100) peak are weaker than that of GNS, implying less restacking and agglomeration of GNS in composites [35]. In comparison, all diffraction peaks observed in $\text{Co}_3\text{O}_4/12.3\%$ GNS composite were still in good accordance with those of cubic spinel Co_3O_4 .

Figure 2 presents the FT-IR spectra of the as-prepared samples. The intensive characteristic peaks of GO, consisting of O–H stretching mode at $3,450\text{ cm}^{-1}$ and C=O stretching vibrations of carboxyl groups at $1,730\text{ cm}^{-1}$, disappear in the spectrum of GNS. The result indicates that the major oxygen-containing functional groups of GO have been removed after reduction [36]. The remaining absorption at around $1,600$ and $1,060\text{ cm}^{-1}$ can be assigned to skeletal vibrations of un-oxidized graphite domains and C–O

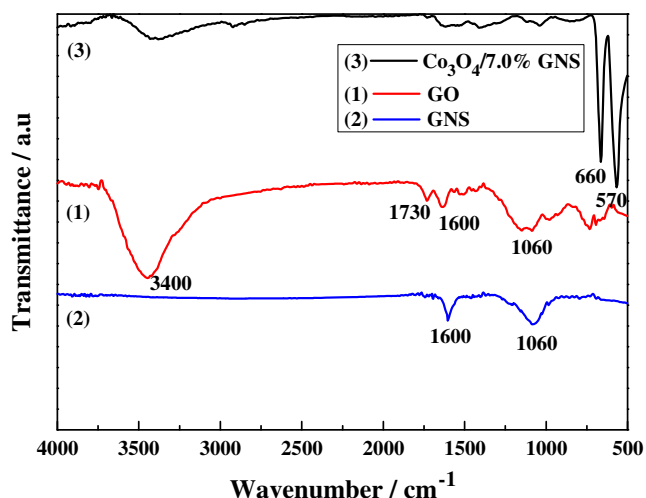


Fig. 2 FT-IR spectra of GNS, GO, and $\text{Co}_3\text{O}_4/7.0\%$ GNS composite

stretching vibrations of the residual epoxy groups, respectively. For the composite, the absorption peaks at 570 and 660 cm^{-1} is attributed to the vibration of the Co–O [37].

The morphology and microstructure of $\text{Co}_3\text{O}_4/7.0\%$ GNS composites are shown in Fig. 3. The cross-sectional AFM images in Fig. 3a, b provide evidence that single-atom layer GO sheet and GNS were obtained with the thickness of 0.80 and 3.54 nm, respectively. The GNS exhibits interconnected 3D porous network in SEM image (Fig. 3c) and crumpled silk-like structure in TEM image (Fig. 5a). Figure 3d–f shows the SEM images and corresponding EDS pattern of $\text{Co}_3\text{O}_4/7.0\%$ GNS composite. As can be seen, the irregular and thin plates with a length of $0.5\text{--}1\text{ }\mu\text{m}$ and width of $100\text{--}300$ nm are decorated on the surface of graphene nanosheets, which could prevent the restacking of graphene nanosheets. The EDS pattern of $\text{Co}_3\text{O}_4/7.0\%$ GNS composite confirms the existence of the elements including Co, O, and C on the surface of graphene nanosheets. For the $\text{Co}_3\text{O}_4/4.1\%$ GNS composite, many stacked irregular platelets were observed in the image (Fig. 4a). It is hard to see scrolled graphene nanosheets. When the content of graphene in composite is 12.3% , the graphene nanosheets agglomerate to form clusters (Fig. 4b). Few cobalt oxide nanoflakes were loosely decorated on the graphene nanosheets.

To investigate the structural information of Co_3O_4 nanoplates on graphene nanosheets, TEM, high-resolution transmission electron microscopy (HRTEM), and selected area electron diffraction (SAED) results are presented in Fig. 5. TEM image in Fig. 5b shows the porous nanoplates consisting of particles with a diameter of around $5\text{--}20$ nm which is probably because of the elimination of H_2O molecules during calcination [38]. It can be obviously observed that Co_3O_4 nanoplates are wrapped by graphene sheets. The SAED pattern in the inset of Fig. 5c reveals the polycrystalline nature of the nanoplates. HRTEM image (as presented in Fig. 5d) shows a clear cubic lattice. The HRTEM image is recorded through the $(-1\ 1\ 2)$ direction. The $(2\text{--}2\ 2)$ and $(2\ 2\ 0)$ lattice spacing are 0.233 and 0.286 nm, respectively. By using the formula for a cubic lattice: $a_0=d(h^2+k^2+l^2)^{1/2}$, a_0 is calculated to be 0.808 nm, corresponding to the given value in the JCDs 43–1003 card [39].

For Raman spectroscopy, the G band at around $1,590\text{ cm}^{-1}$ represents the E_{2g} phonons of C sp^2 atom, while the D band at around $1,330\text{ cm}^{-1}$ is breathing modes of rings or K-point phonons of A_{1g} symmetry. In general, the I_D/I_G intensity ratio reflects the disorder density of carbon materials [40]. Figure 6 shows the Raman spectra of GO, GNS, and $\text{Co}_3\text{O}_4/7.0\%$ GNS composite in the range from 400 to $2,000\text{ cm}^{-1}$. The intensity ratio (I_D/I_G) of GO is 0.962 . Compared with GO, the I_D/I_G of GNS is increased to 1.236 due to the unrepaired defects after the removal of

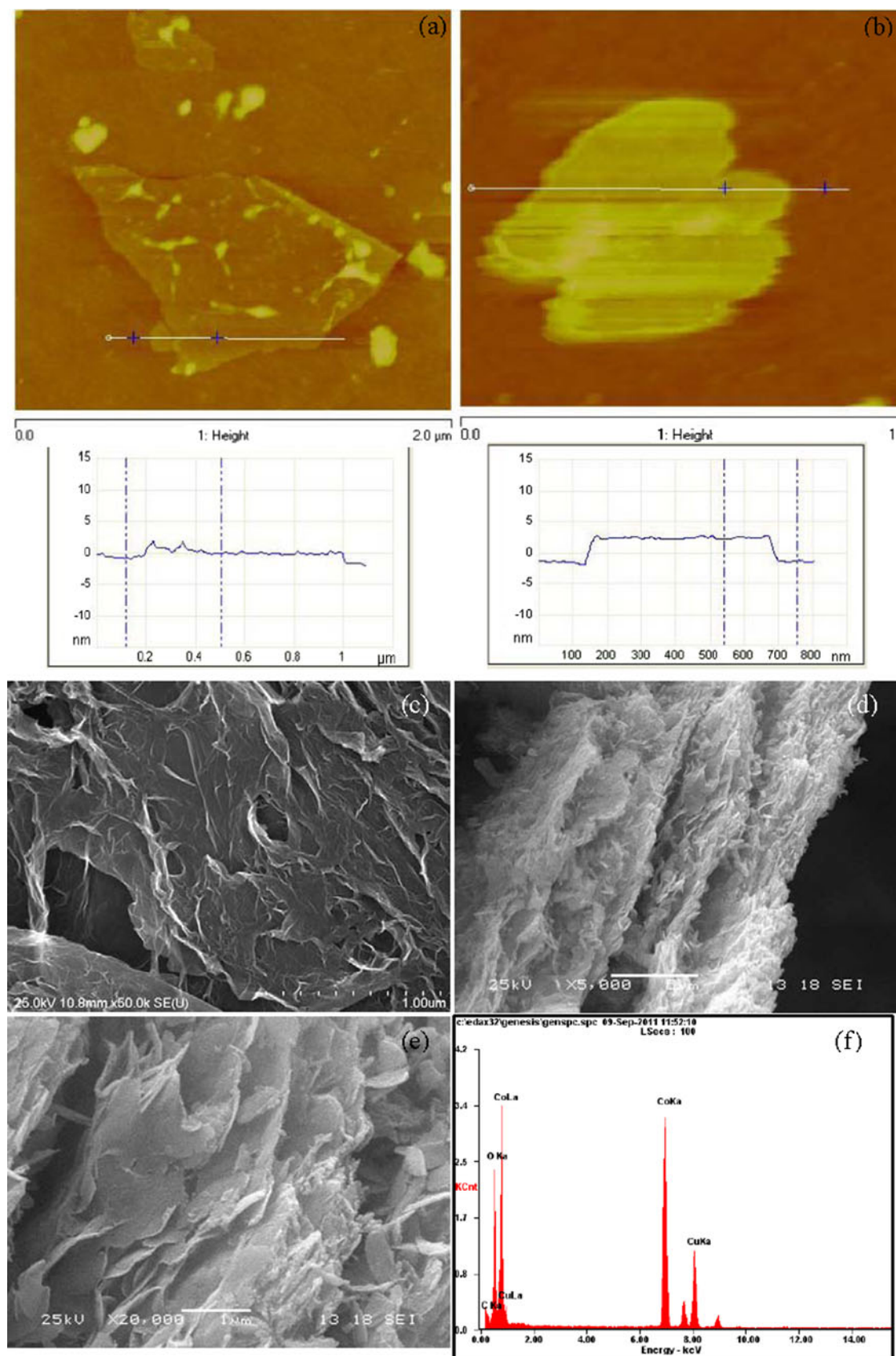
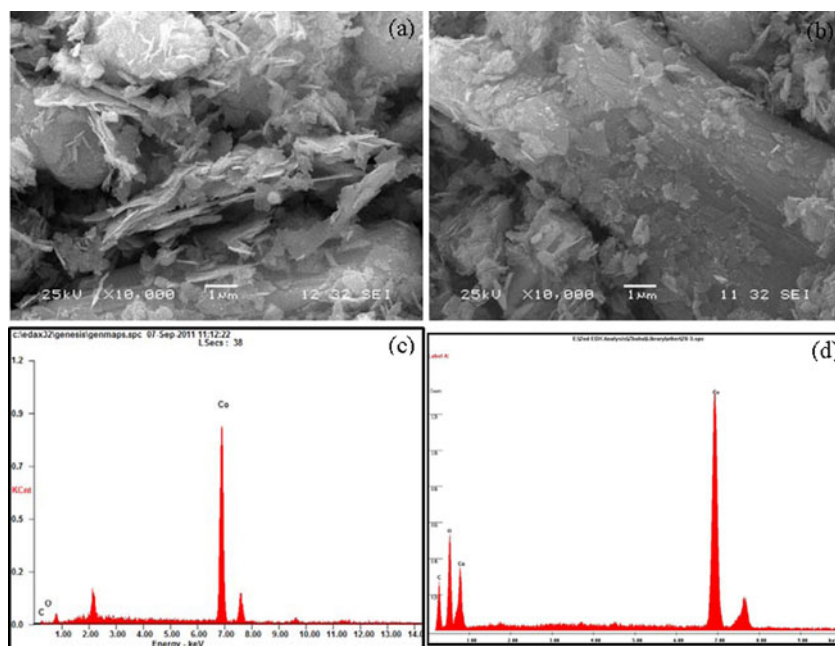


Fig. 3 **a** AFM image and cross-section analysis of GO and **b** GNS; **c** SEM image of GNS prepared by hydrothermal method; **d**, **e** SEM image and **f** corresponding EDS pattern of Co₃O₄/7.0 % GNS composite

Fig. 4 SEM image of **a** Co_3O_4 /4.1 % GNS composite and **b** Co_3O_4 /12.3 % GNS composite; corresponding EDS pattern of **c** Co_3O_4 /4.1 % GNS composite and **d** Co_3O_4 /12.3 % GNS composite



oxygen-containing functional groups, which leads to destruction of sp^2 network [41]. For Co_3O_4 /7.0 % GNS composite, the I_D/I_G is 1.247 and the additive peaks were detected at around 191, 476, 518, and 680 cm^{-1} , which can be attributed to E_g , E_{2g}^1 , F_{2g}^2 , and A_{1g} modes of Co_3O_4 [42].

According to the results presented earlier, the formation processes of Co_3O_4 nanoplates/GNS composite is proposed in Fig. 7. Previous studies have indicated that the oxygen functional groups such as epoxy and hydroxyl decorates on GO sheets, and the carbonyl and carboxyl groups are presumably located at the edges. After the treatment in

TMAOH aqueous solution, the GO sheets are exfoliated by the intercalation of TMA^+ into the interlayer of GO and negatively charged through the ion exchange of OH^- to H^+ from carboxyl [43]. The metal ions (Co^{2+}) are adsorbed onto the surface of GO sheets due to the electrostatic force, and cobalt hydroxide was grown on the surface accompanied with the reduction of GO to graphene under a hydrothermal treatment. Because of the removal of water molecules during calcination, the cobalt oxide nanoplates become porous, which is beneficial for permeating of electrolyte. Co_3O_4 nanoplates are firmly attached to the nanosheets of graphene, which could effectively prevent the restacking of

Fig. 5 **a** TEM image of GNS, **b** TEM image of Co_3O_4 nanoplates obtained from the composites after agitation for 1 h; **c**, **d** TEM image of Co_3O_4 /7.0 % GNS composite; **e** HRTEM image of the Co_3O_4 nanoparticle surface viewed from the broad plane. The insets in **c** and **d** show the corresponding SAED pattern and fast Fourier transform pattern

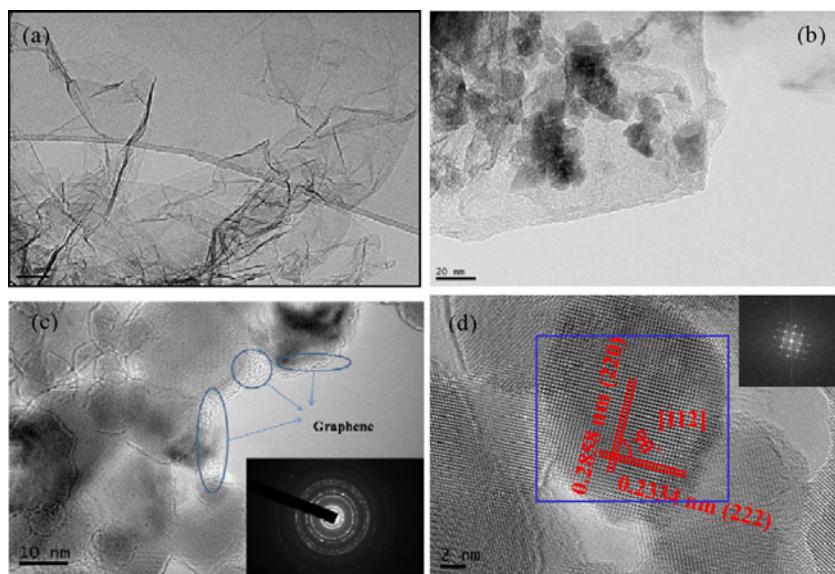


Fig. 6 Raman spectra of GNS, GO, and $\text{Co}_3\text{O}_4/7.0\%$ GNS composite

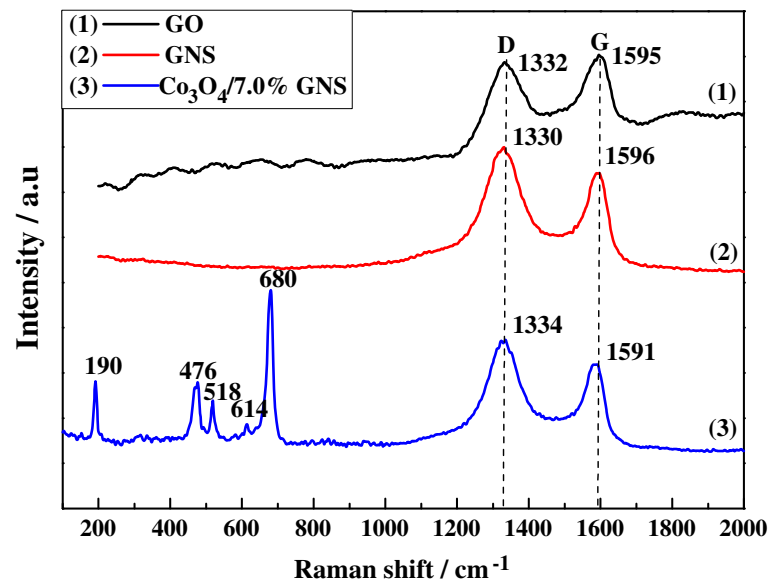
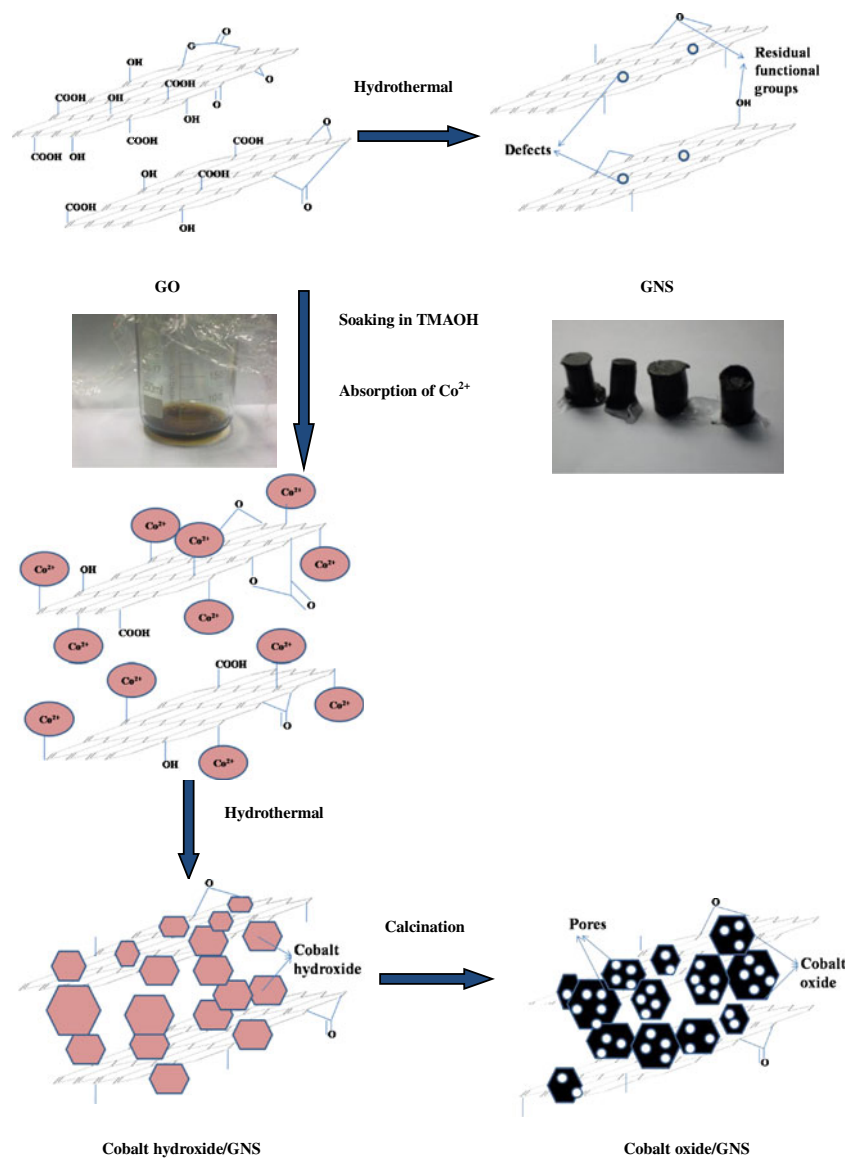


Fig. 7 Schematic illustration of the formation process of Co_3O_4 nanoplates/GNS composite

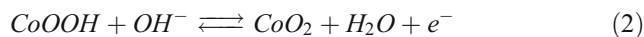
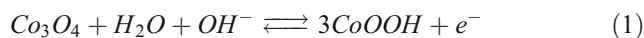


graphene nanosheets. Meanwhile, the volume expansion of Co_3O_4 could also be restrained, suggesting that the Co_3O_4 nanoplates/GNS composite may show good electrochemical performance.

Electrochemical properties

Figure 8a displays the CV curves of $\text{Co}_3\text{O}_4/7.0\%$ GNS composite at various scan rates of 5, 10, 20, and 50 mV s^{-1} . The CV curves are different from the ideal rectangular shape of the typical electric double-layer capacitance. There are a couple of redox peaks at about 0.21 and 0.37 V (vs SCE) similar to that of pure Co_3O_4 , which suggest that the capacitance is mainly from the pseudocapacitance of Co_3O_4 . The peaks are related to the reactions between different

oxidation states of Co according to the following equations [44, 45]:



With the increasing rates, the anodic peaks shift toward positive potential and the cathodic peaks shift toward negative potential. The potential difference between anodic and cathodic peak materials is around 0.16 V at a scan rate of 5 mV s^{-1} . The coulombic efficiency of electrode calculated from the ratio of discharge time to charge time is 92.8 % at the specific current of 1.25 A g^{-1} . These two factors indicate the quasi-reversible feature of redox couples [38]. Furthermore, the specific current increases from 5 to 50 mV s^{-1} , which indicates fast redox reaction. For comparison, CV curves for $\text{Co}_3\text{O}_4/7.0\%$ GNS composite, pure Co_3O_4 nanoplates, and GNS at 10 mV s^{-1} are shown in Fig. 8b. The internal area of CV curve for $\text{Co}_3\text{O}_4/7.0\%$ GNS composite is apparently larger than that of pure Co_3O_4 nanoplates, implying that the specific capacitance of composite is higher than that of pure Co_3O_4 nanoplates. In addition, the CV curve of GNS is almost ideally rectangular, exhibiting the electric double-layer capacitance of GNS [33].

The specific capacitance (SC), based on galvanostatic charge/discharge measurement, can be calculated from the following equation:

$$\text{SC}_{\text{CD}} = \frac{I \times t}{m \times \Delta V} \quad (3)$$

where I is the discharge current (A), t is the discharge time (s), m is the mass of the electrode materials (g), and V is the discharging potential range.

As shown in Fig. 9a, the discharge curves consist of a sudden potential drop from 0.4 to 0.3 V and a slow potential decay from 0.3 to 0.2 V. It is in good agreement with results corresponding to CV curves. The charge–discharge curve of GNS is presented in Fig. 9b. The voltage decreases linearly along the discharge time, which shows ideal double-layer capacitive behavior. According to Eq. (3), the specific capacitance of $\text{Co}_3\text{O}_4/7.0\%$ GNS composite is calculated to be 703.4, 667.9, 472.5, 412.5, and 385.1 F g^{-1} at the current density of 0.625, 1.25, 2.5, 5.0, and 12.5 A g^{-1} , respectively. Compared to 334.2 F g^{-1} for pure Co_3O_4 nanoplates and 224.2 F g^{-1} for GNS at 0.5 A g^{-1} , the capacitance of the composite is remarkably enhanced, which is also higher than Co_3O_4 /graphene materials prepared by microwave-assisted method (243.3 F g^{-1}) [28] and surfactant-assisted synthesized Co_3O_4 /reduced graphene oxide (163.8 F g^{-1}) [46]. The remarkable enhancement in specific capacitance is attributed to the unique properties of the Co_3O_4 /GNS composite, shown as follows: (1) the graphene nanosheets

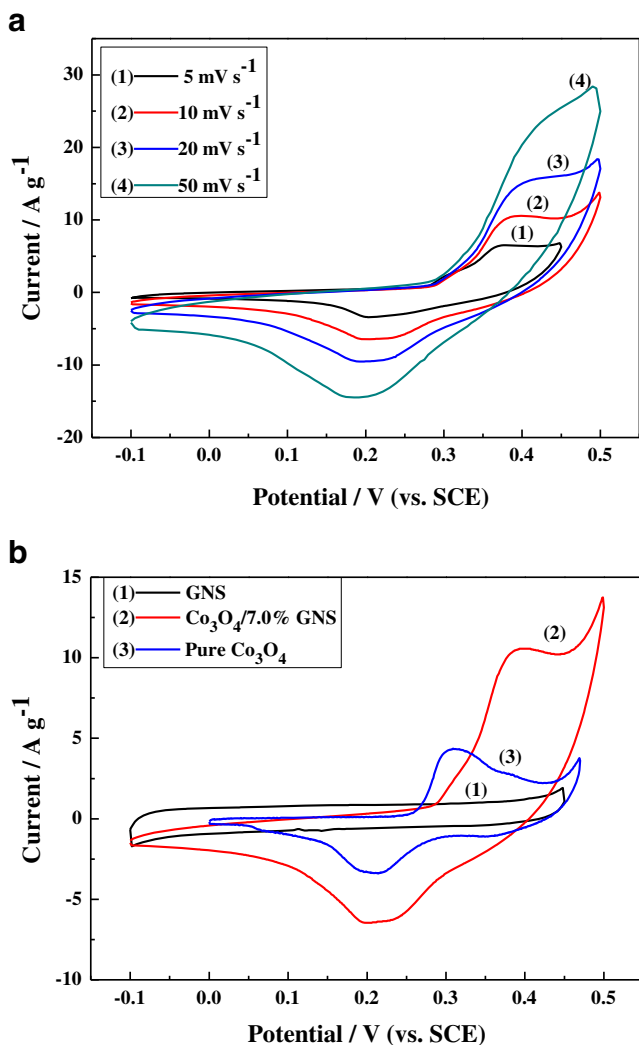


Fig. 8 **a** Cyclic voltammograms of $\text{Co}_3\text{O}_4/7.0\%$ GNS composite electrode in 2 M KOH solution at various scan rates. **b** Cyclic voltammograms of GNS, pure Co_3O_4 nanoplates, and $\text{Co}_3\text{O}_4/7.0\%$ GNS composite electrodes in 2 M KOH solution at a scan rate of 10 mV s^{-1}

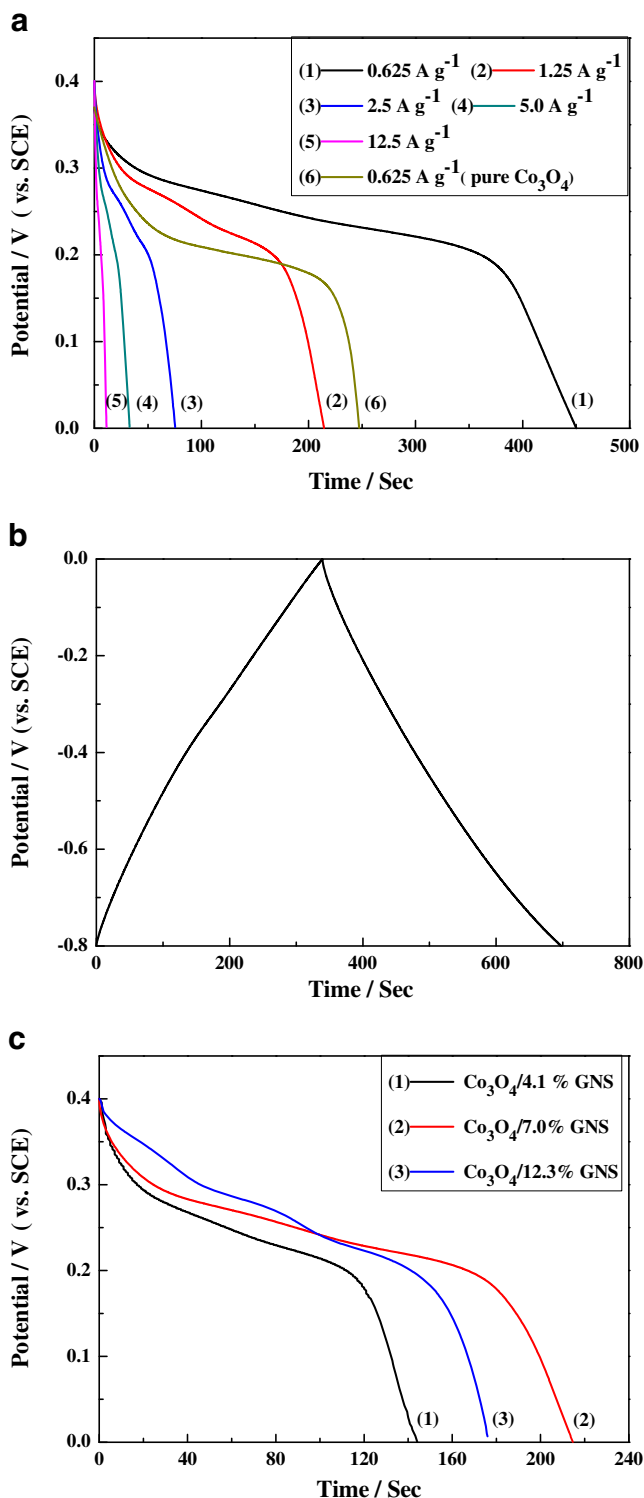


Fig. 9 **a** Galvanostatic discharge curves of pure Co_3O_4 nanoplates and $\text{Co}_3\text{O}_4/7.0\%$ GNS composite electrodes in 2 M KOH solution at different current densities. **b** Galvanostatic charge-discharge curves of GNS electrode in 6 M KOH solution at a current density of 0.5 A g^{-1} . **c** Galvanostatic discharge curves of $\text{Co}_3\text{O}_4/\text{GNS}$ composites with the graphene content of 4.1, 7.0 and 12.3% in 2 M KOH solution at a current density of 1.25 A g^{-1}

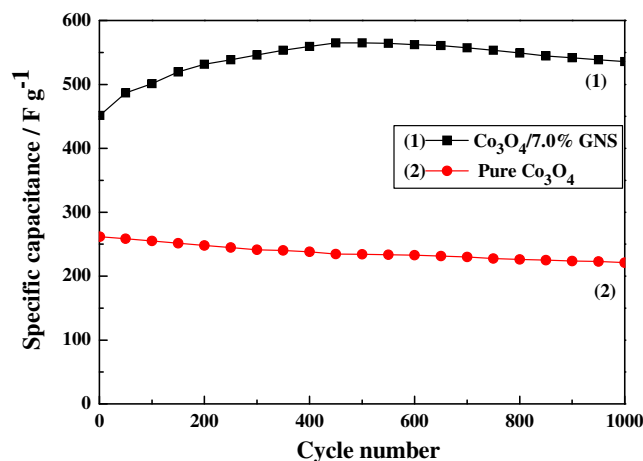


Fig. 10 Cycling performances of $\text{Co}_3\text{O}_4/7.0\%$ GNS composites and pure Co_3O_4 nanoplates under a current density of 2.5 A g^{-1}

provide a large surface for well-anchored Co_3O_4 nanoplates and a highly conductive network for electron transport; (2) the Co_3O_4 nanoplates inhibit the restacking of graphene, improving the absorption of electrolyte on the surface of electrode; and (3) the channel between graphene and Co_3O_4 nanoplates facilitates ion transportation [47].

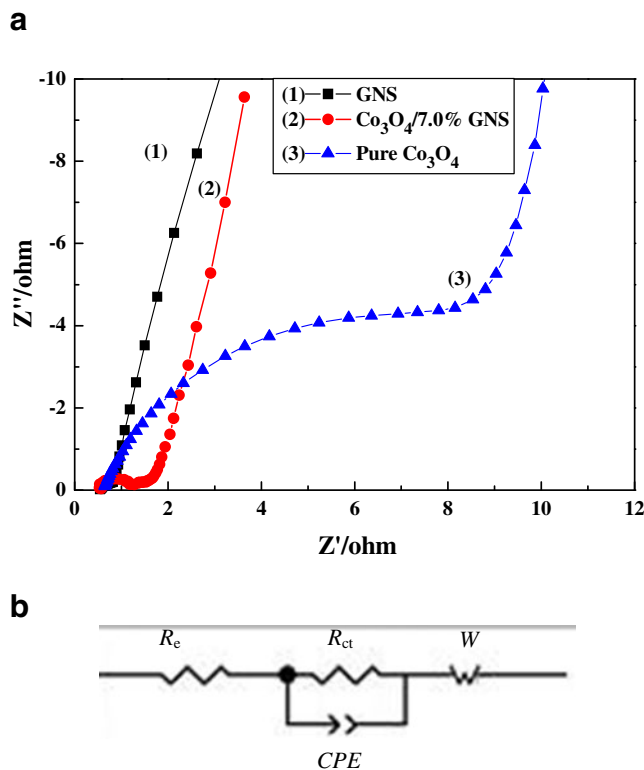


Fig. 11 **a** Nyquist plots of GNS, pure Co_3O_4 nanoplates, and $\text{Co}_3\text{O}_4/7.0\%$ GNS composites electrodes; **b** the equivalent circuit for the EIS of $\text{Co}_3\text{O}_4/7.0\%$ GNS electrode composites

To further understand the effect of graphene mass ratio on specific capacitance, the galvanostatic charge/discharge curves of $\text{Co}_3\text{O}_4/\text{GNS}$ composites with the graphene content of 4.1, 7.0, and 12.3 % at 1.25 A g^{-1} are presented in Fig. 9c. The $\text{Co}_3\text{O}_4/7.0 \%$ GNS composite shows maximum capacitance, which is attributed to a unique morphology that can be observed from the SEM. When the graphene loading is less than 7.0 %, the graphene does not effectively improve the conductivity of composite and it would result to the low utilization of Co_3O_4 nanoplates. When the graphene content is more than 7.0 %, the graphene nanosheets agglomerate with each other, which could lead to the decrease of specific surface and electroactive site [48].

To investigate the long cycling performance of $\text{Co}_3\text{O}_4/7.0 \%$ GNS composite and pure Co_3O_4 nanoplates, the charge–discharge tests were performed at 2.5 A g^{-1} for 1,000 cycles (Fig. 10). The special capacitance of $\text{Co}_3\text{O}_4/\text{GNS}$ composite is increased by 25.2 % after 450 cycles. In the following 550 cycles, only slight capacitance loss could be observed. After 1,000 cycles, the capacitance still increases to 18.7 % of the initial capacitance. During cycling, flexible GNS can inhibit the volume change and detachment of Co_3O_4 nanoplates [28]. It is noted that the specific capacitance of the composite is gradually increased. This phenomenon could be attributed to the reasons as follows: At the initial cycle, the nanostructures wrapped by graphene have not been fully activated. After continual charge/discharge cycling, the electrochemical active sites will be fully exploited to the electrolyte [15, 49]. For pure Co_3O_4 nanoplates, the capacitance fading is 15.2 % after 1,000 cycles.

In order to evaluate the effect of graphene in electrode materials, EIS measurement was performed at 0.1 V in the frequency range of 0.01 to 10^5 Hz. The Nyquist impedance plots of three electrodes (Fig. 11) exhibit a semicircle at high frequency and a straight line at low frequency. At very high frequency, the crossover point of the semicircle on the real part is a combinational resistance of the electrolyte resistance, intrinsic resistance of substrate, and contact resistance between the active materials and current collector (R_c) [50]. The values of R_c are about 0.5Ω , almost the same for three electrodes. Meanwhile, the semicircle corresponds to a parallel RC element, the charge transfer resistance (R_{ct}), and the constant phase capacitance [49]. With the intercalation of graphene, the R_{ct} decreased from 8.38 to 0.98Ω obviously. The straight line in low frequency represents the Warburg resistance (W) related to the electrolyte diffusion process and OH^- ion diffusion into electrode [51]. The almost vertical shape, indicating fast diffusion of ions in electrolyte during charge/discharge process, is an ideally capacitive behavior [52].

Conclusions

A series of Co_3O_4 nanoplates/graphene nanosheet composites has been prepared by a facile and green hydrothermal reduction–thermal decomposition method. GNS effectively restrain the volume expansion of Co_3O_4 nanoplates during cycling and improve the conductivity of electrode, whereas the Co_3O_4 nanoplates prevent the restacking of GNS. Among the composites, the $\text{Co}_3\text{O}_4/7.0 \%$ GNS composite exhibits excellent electrochemical performance with the highest specific capacitance and long cycling life. The special capacitance of 703.4 F g^{-1} is achieved at a current density of 0.625 A g^{-1} . Even at 12.5 A g^{-1} , 385.1 F g^{-1} is retained with the retention of 63 %. After 1,000 cycles, the increase of capacitance is 18.7 % of the initial value.

Acknowledgments This work was supported by National Natural Science Foundation of China (no. 50972165) and Nonferrous Metal Research Fund of Hunan Province Nonferrous Group (no. Y2008-01-007).

References

1. Conway BE (1999) Electrochemical supercapacitors, scientific fundamentals and technological applications. Kluwer Academic, New York
2. Simon P, Gogotsi Y (2008) Nat Mater 7:845–854
3. Hu CC, Chang HK, Lin MC, Wu YT (2006) Nano Lett 6:2690–2695
4. Yang GW, Xu GL, Li HL (2008) Chem Commun 44:6537–6539
5. Wang HQ, Li ZS, Yang JH, Li QY, Zhong XX (2009) J Power Sources 194:1218–1221
6. Wang DW, Li F, Liu M, Lu GQ, Cheng HM (2008) Angew Chem Int Ed 47:373–376
7. Chen Z, Qin YC, Weng D, Xiao QF, Peng YT, Wang XL, Li HX, Wei F, Lu YF (2009) Adv Funct. Mater 19:3420–3426
8. Zhang XJ, Shi WH, Zhu JX, Kharistal DJ, Zhao WY, Lalia BS, Hng HH, Yan QY (2011) ACS Nano 5:2013–2019
9. Lang JW, Yan XB, Xue QJ (2011) J Power Sources 196:7841–7846
10. Wang Y, Zhang HJ, Lu L, Stubbs LP, Wong CC, Lin JY (2010) ACS Nano 4:4753–4761
11. Wang JG, Yang Y, Huang ZH, Kang FY (2011) Electrochim Acta 56:9240–9247
12. Wang HL, Casalongue HS, Liang YY, Dai HJ (2010) J Am Chem Soc 132:7472–7477
13. Chen S, Zhu JW, Wang X (2010) J Phys Chem C 114:11829–11834
14. Wang L, Wang DL (2011) Electrochim Acta 56:5010–5015
15. Gao Z, Wang J, Li ZS, Yang WL, Wang B, Hou MJ, He Y, Liu Q, Mann T, Yang PP, Zhang ML, Liu LH (2011) Chem Mater 23:3509–3516
16. Novoselov KS, Geim AK, Morozov SV, Jiang D, Zhang Y, Dubonos SV, Grigorieva IV, Firsov AA (2004) Science 306:666–669
17. Yoo EJ, Kim JD, Hosono E, Zhou HS, Kudo T, Honma I (2008) Nano Lett 8:2277–2282
18. Qu LT, Liu Y, Beak JB, Dai LM (2010) ACS Nano 4:1321–1326
19. Wang X, Zhi LJ, Müllen K (2008) Nano Lett 8:323–327

20. Liu CG, Yu ZN, Neff D, Zhamu A, Jang BZ (2010) *Nano Lett* 10:4863–4868
21. Zhu YW, Murali S, Stoller MD, Ganesh KJ, Cai WW, Ferreira PJ, Pirkle A, Wallace DM, Cychosz KA, Thommes M, Su D (2011) *Science* 332:1537–1541
22. Stoller MD, Park SJ, Zhu YW, An JH, Ruoff RS (2008) *Nano Lett* 8:3498–3502
23. Wang B, Park JS, Wang CY, Ahn HJ, Wang GX (2010) *Electrochim Acta* 55:6812–6817
24. Yan J, Fan ZJ, Wei T, Qian WZ, Zhang ML, Wei F (2010) *Carbon* 48:3825–3833
25. Zhang JT, Jiang JW, Zhao XS (2011) *J Phys Chem C* 115:6448–6454
26. Chen YL, Hu ZA, Chang YQ, Wang HW, Zhang ZY, Yang YY, Wu HY (2011) *J Phys Chem C* 115:2563–2571
27. Lu T, Zhang Y, Li H, Pan L, Li Y, Sun Z (2010) *Electrochim Acta* 55:4170–4173
28. Yan J, Wei T, Qiao WM, Shao B, Zhao QK, Zhang LJ, Fan ZJ (2010) *Electrochim Acta* 55:6973–6978
29. Deng MJ, Huang FL, Sun IW, Tsai WT, Chang JK (2010) *Nanotechnology* 20:175602–175607
30. Kim HY, Seo DH, Kim SW, Kim JS, Kang KS (2011) *Carbon* 49:326–332
31. Li BJ, Cao HQ, Shao J, Li GQ, Qu MZ, Yin G (2011) *Inorg Chem* 50:1628–1632
32. Hummers WS, Offinan RE (1958) *J Am Chem Soc* 80:1339
33. Xu YX, Sheng KX, Li C, Shi GQ (2010) *ACS Nano* 4:4324–4330
34. Liu ZH, Wang ZM, Yang X, Ooi K (2002) *Langmuir* 18:4926–4932
35. Wu ZS, Ren WC, Wen L, Gao LB, Zhao JP, Chen ZP, Zhou GM, Li F, Cheng HM (2010) *ACS Nano* 4:3187–3194
36. Zhang WN, He W, Jing XL (2010) *J Phys Chem B* 114:10368–10373
37. Dong Z, Fu YY, Han Q, Xu YY, Zhang H (2007) *J Phys Chem B* 111(50):18475–18478
38. Kong LB, Lang JW, Liu M, Luo YC, Kang L (2009) *J Power Sources* 194:1194–1201
39. He T, Chen DR, Jiao XL, Wang YL (2006) *Adv Mater* 18:1078–1082
40. Kudin KN, Ozbas B, Schnlepp HC (2008) *Prud'homme RK, Aksay IA, Car R. Nano Lett* 8:36–41
41. Gao W, Alemany LB, Ci L, Ajayan PM (2009) *Nat Chem* 1:403–408
42. Liu HC, Yen SK (2007) *J Power Source* 166:478–484
43. Li HJ, Zhu G, Liu ZH, Yang ZP, Wang ZL (2010) *Carbon* 48:4391–4396
44. Svegl F, Orel B, Mutchins MG, Kalcher K (1996) *J Electrochem Soc* 143:1532–1539
45. Lin C, Ritter JA, Popov BN (1998) *J Electrochem Soc* 145:4097–4103
46. Zhou WW, Liu JP, Chen T, Tan KS, Jia XT, Liu ZQ, Cong CX, Yang HP, Li CM, Yu T (2011) *Phys Chem Chem Phys* 13:14462–14465
47. Zhou GM, Wang DW, Li F, Zhang LL, Li N, Wu ZS, Wen L, Lu GQ, Cheng HM (2010) *Chem Mater* 22:5306–5313
48. Zhang LJ, Zhang XG, Shen LF, Gao B, Hao L, Lu XJ, Zhang F, Ding B, Yuan CZ (2012) *J Power Sources* 199:395–401
49. Wang HW, Hu ZA, Chang YQ, Chen YL, Wu HY, Zhang ZY, Yang YY (2011) *J Mater Chem* 21:10504–10511
50. Wu MS, Hsieh HH (2008) *Electrochim Acta* 53:3427–3435
51. Li YH, Huang KL, Liu SQ, Yao ZF, Zhuang SX (2011) *J Solid State Electrochem* 15:587–592
52. Di Fabio A, Giogori A, Mastragostino M, Soavi F (2001) *J Electrochem Soc* 148:A845–A850